Geothermal reservoir characterization using distributed temperature sensing at Brady Geothermal Field, Nevada

Jeremy R. Patterson[1], Michael Cardiff[1], Thomas Coleman[2], Herb Wang[1], Kurt L. Feigl[1], John Akerley[3], and Paul Spielman[3]

Abstract

Distributed temperature sensing (DTS) systems provide near real-time data collection that captures borehole spatiotemporal temperature dynamics. Temperature data were collected in an observation well at an active geothermal site for a period of eight days under geothermal production conditions. Collected temperature data showcase the ability of DTS systems to detect changes to the location of the steam-water interface, visualize borehole temperature recovery — following injection of a cold-water "slug" — and identify anomalously warm and/or cool zones. The high sampling rate and spatial resolution of DTS data also shows borehole temperature dynamics that are not captured by traditional pressure-temperature survey tools. Inversion of thermal recovery data using a finite-difference heat-transfer model produces a thermal-diffusivity profile that is consistent with laboratory-measured values and correlates with identified lithologic changes within the borehole. Used alone or in conjunction with complementary data sets, DTS systems are useful tools for developing a better understanding of both reservoir rock thermal properties as well as within and near borehole fluid movement.

Introduction

Understanding the temperature profile in geothermal boreholes is a first step in determining thermal properties immediately surrounding the borehole. Thermal characterization of geothermal reservoirs is a critical component of decision making and predictive modeling of reservoir production potential. Temperature is considered one of the most critical state variables of a reservoir as it directly influences production potential and informs decisions regarding well installation depth, casing length, and other operational considerations. In addition, understanding changes to pressures or water levels in wells over time can help assess hydraulic connectivity between different reservoir intervals.

Plant managers commonly monitor the average temperature of pumped water at production and injection wellheads. In addition, vertical logs of temperature variability are commonly collected by pressure-temperature (P-T) survey, which involves lowering and raising a temperature probe through the borehole and recording temperature and pressure at specified depth intervals. Temperature logs provide power-plant operators with a snapshot of the temperature profile at discrete times, requiring that multiple P-T surveys be conducted at regular intervals in an effort to understand reservoir temperature evolution under normal operating conditions.

Fiber-optic distributed temperature sensing (DTS) is a well-established monitoring technology in the hydrologic sciences. Following successful studies demonstrating the use of DTS in identifying and/or quantifying groundwater-surface water exchanges, researchers have adopted this tool to gain a better understanding of borehole hydrogeology. Bense et al. (2016) conducted a thorough review of shallow borehole studies using DTS systems to better understand borehole groundwater dynamics. Read et al. (2013) and Leaf et al. (2012) used DTS in open boreholes to determine areas of fracture flow by using heat as a tracer through thermal dilution testing. Read et al. (2015) and Sellwood et al. (2015) used DTS in conjunction with a point heating element to determine vertical velocities within open boreholes. While previous studies have focused on flow within open boreholes, Coleman et al. (2015) used DTS to determine fracture flow within lined boreholes under natural-gradient conditions. Freifeld et al. (2008) illustrated the use of borehole DTS to determine thermal conductivity of permafrost immediately surrounding the borehole. They utilized an electrical heating element in the borehole to create a temperature transient, which was analyzed during inversion to determine thermal conductivity.

Despite the numerous studies illustrating the use of DTS in open boreholes, there is limited literature surrounding its use in a geothermal setting. As an example, Sakaguchi and Matsushima (2000) demonstrated the use of DTS to determine the location of fractures within boreholes using cold-water injection at an active geothermal site. Ikeda et al. (2000) used DTS during well completion at a geothermal site to monitor borehole temperature recovery after drilling completion and vertical-flow profiling. These prior two studies limited data analysis to qualitative interpretations of individual snapshots from borehole temperature profiles. We are unaware of any existing peer-reviewed studies in the literature that illustrate the capability of DTS to show natural borehole dynamics or investigate its usage in a geothermal setting in a quantitative manner.

In this study, we demonstrate the utility of installing fiber-optic DTS systems in an observation borehole at an active geothermal power plant. We illustrate the ability of DTS to capture spatiotemporal dynamics during borehole temperature recovery following injection of a cold-water slug. Last, we develop a numerical heat-transfer model, which is used to estimate variability in reservoir thermal diffusivity (i.e., the ratio of thermal conductivity to volumetric heat capacity) of reservoir rock near the observation well using a simple parameter-estimation approach. Our inversion strategy is a modified version of the methodology employed by Freifeld et al. (2008), where the temperature within the borehole is perturbed from equilibrium. We then use the temperature recovery to estimate a depth profile of thermal diffusivity in 1 m increments throughout the cased and fluid-filled portion of the borehole. Our methodology differs in that we do not use electrical current to initiate the temperature change. Instead, we use a

[1]University of Wisconsin-Madison.
[2]Silixa LLC.
[3]ORMAT Technologies Inc.

https://doi.org/10.1190/tle36121024a1.1.

cold-water slug to decrease the borehole temperature and prompt heat diffusion from the reservoir into the borehole.

Study area

Brady Geothermal Field — henceforth referred to simply as "Brady" — is a geothermal field located near Fernley, Nevada, within the Basin and Range Province of the United States. It is located on the Brady fault zone, which is a prominent north–northeast-striking normal fault system approximately 4 km in length. Production wells access the reservoir up to depths of approximately 2 km in a prominent fault stepover with a high density of faulting, as seen in Figure 1. Reinjection wells access the subsurface at much shallower depths of 100–200 m, and are separated from production wells by approximately 2 km across the land surface (Siler et al., 2016; Feigl and Team, 2017). During the "PoroTomo" field experiment in March 2016, several wells that were no longer used for production were used as observation wells to record borehole pressures and temperatures (Feigl and Team, 2017).

A well schematic for Brady observation well 56-1, the primary well examined in this study, shows lithology with depth, casing diameter, screened interval, water level, temperature depth profile, and prominent faults detected during drilling (Figure 2). This schematic is based on a compilation of well construction reports, lithology maps from current geologic models for Brady, and measurements obtained during P-T surveys of the well. The lithologic profile is based on current 3D geologic and structural modeling and is representative of the lithology seen throughout the geothermal field (Siler et al., 2016). The surficial geology is dominated by alluvial fans composed primarily of volcanic sediments. Deeper lithologies are composed of undifferentiated lacustrine units, limestones, and crystalline basement rocks composed of basalts and andesites (Siler et al., 2016). Fluid flow through the reservoir is assumed to be fault dominated since these rocks have low permeability and several fumaroles are oriented parallel to the Brady fault system (Siler et al., 2016; Feigl and Team, 2017). The fault system channels fluids from the shallow aquifer to the deeper reservoir (Ali et al., 2016).

Methods

The DTS data described in this work are one portion of data collected during the DOE-funded PoroTomo field experiment, a collaborative effort between the University of Wisconsin-Madison and several other institutions, designed to test integrated technologies for characterizing critical properties of geothermal reservoirs (Feigl and Team, 2017). The PoroTomo integrated field experiment follows from earlier observations of subsidence and surface deformation at Brady (Ali et al., 2016) and was conducted over a period of four weeks during March 2016. The PoroTomo team collected geophysical and hydrologic data to characterize rock properties in a 500 × 1500 × 400 m

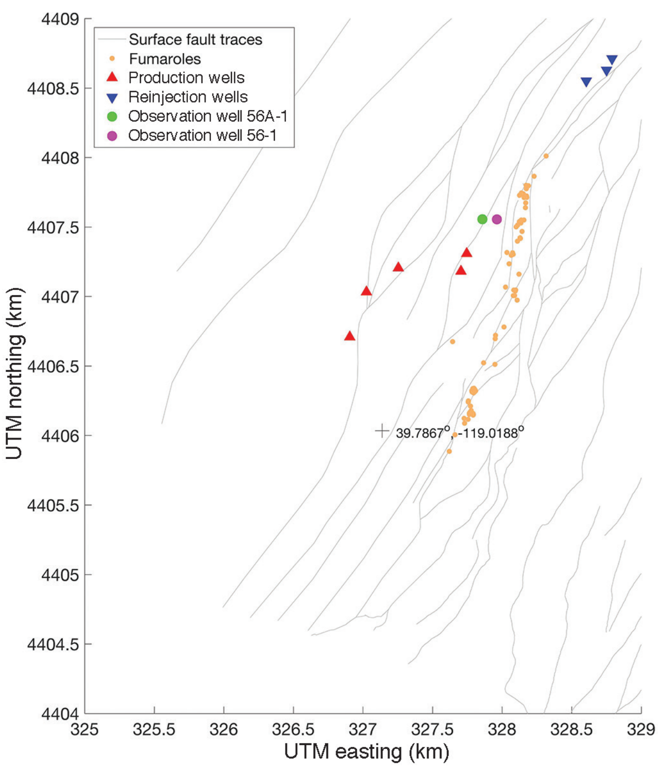

Figure 1. Plan view map of Brady Geothermal Field near Fernley, Nevada. Identified fiducial point represents location of site well 15-12.

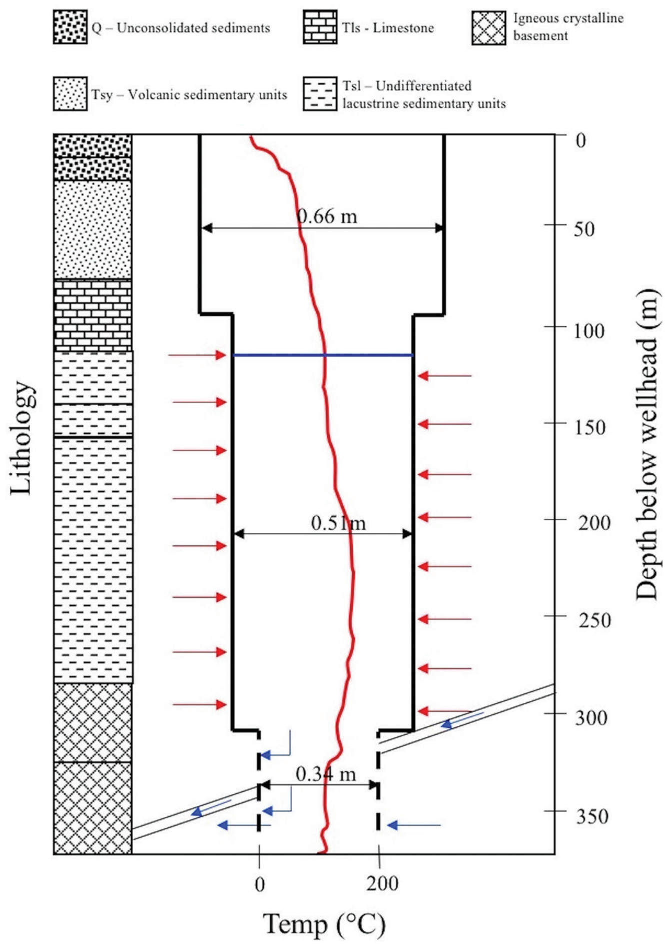

Figure 2. Brady observation well 56-1 construction, lithology, and pre-DTS installation observations. Well construction information provided by ORMAT Inc. Lithology based on a current geologic model (Siler et al., 2016). Temperature profile (red line) based on initial P-T survey. Arrows indicate conceptual model for heat diffusion (red arrows) and water movement (blue arrows). Water level in the well is approximately 120 m below wellhead (blue line).

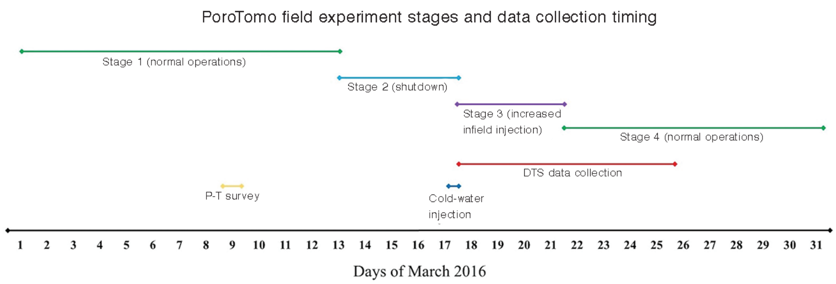

Figure 3. Gantt chart showing stages and timing of the integrated PoroTomo field experiment, period of DTS data collection, date of cold-water slug injection, and date of previous P-T survey.

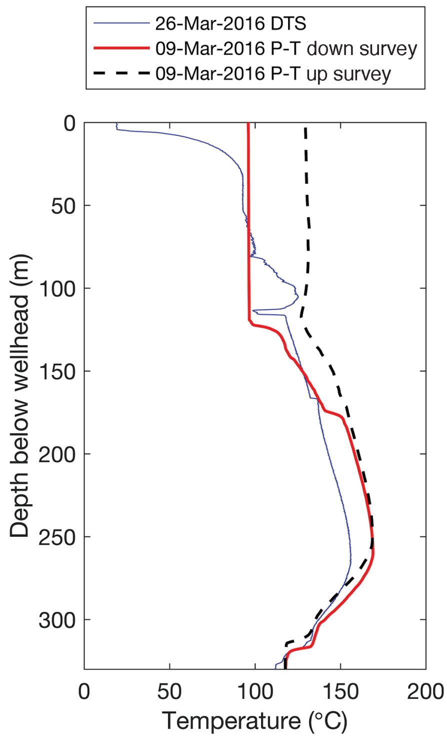

Figure 4. Temperature log in observation well 56-1 at Brady comparing the data provided by traditional logging tools (P-T survey) and DTS systems. The temperature log given by DTS shows identical temperature trends when compared to traditional logging methods. Difference between downgoing and upgoing P-T survey illustrates the effect of thermal inertia on this tool.

volume at a 50 m resolution at Brady (Feigl and Team, 2017). The field experiment consists of four stages based on plant operations: (1) normal plant operations; (2) full plant shutdown; (3) increased infield injection; and (4) resumption of normal plant operations (Figure 3). During each stage of the experiment, the reservoir was monitored by a combination of active and ambient seismic instrumentation (nodal seismometers and distributed acoustic sensing), InSAR satellite passes, dynamic GPS measurements, surface and borehole DTS, and pressure sensors installed in observation wells. This combined instrumentation strategy was designed to monitor the thermal, pressure, and deformation response of the reservoir during changes to site operations. In this paper, we focus solely on individual analysis of the borehole DTS data, which is available at the Geothermal Data Repository (Coleman, 2016).

DTS installation. We used fiber-optic DTS to monitor temperature changes in observation well 56-1 for a period of eight days during stages 3 and 4 of the PoroTomo field experiment. The DTS system deployed at Brady uses Raman optical backscatter technology and the Stokes/anti-Stokes ratio, which is based on photon excitation, to determine distance and temperature, respectively, along the cable. (Bense et al., 2016). This study used a high-resolution ULTIMA-S DTS (Silixa Ltd., Elstree, United Kingdom) with temperature determined using a double-ended calibration configuration. We use an external calibration bath to further refine temperature-offset effects. A full discussion of the Raman backscatter theory and DTS configuration is well documented in the literature and is beyond the scope of this study (Bense et al., 2016).

We used the following process to install the DTS cable. First, for safety reasons, well 56-1 was cooled by injection of a 15 m^3 slug of cold water. This cold-water slug was injected into well 56-1 on 17 March 2016 at approximately 16:00 UTC. Following this, the DTS cable was immediately inserted into the well, to a depth of 372 m below the wellhead. We then connected the cable to a DTS interrogator at the land surface, and began monitoring shortly thereafter. DTS cable installation required approximately three hours, and data collection in well 56-1 began on 17 March 2016 23:25 UTC. Borehole temperature recovery was recorded in near real time with a temporal sampling interval of 60 s. The DTS system collected data every 0.126 m along the cable with an instrument resolution of 0.29 m. We averaged the collected temperature data to 1 m bins for data analysis and inversion.

Data quality verification. The DTS cable installed in this work used a double-ended configuration, which allowed two measurements of temperature to be collected at each observation location. Colocated measurements of temperature by DTS showed little variability with an average difference of less than 0.5°C, suggesting high accuracy. As another measure of data quality, Figure 4 shows temperature logs for well 56-1 as measured by P-T survey prior to DTS installation and a temperature profile measured by DTS during the final day of site monitoring. DTS and P-T survey data show very similar trends in the temperature with depth but there is a noticeable difference in the recorded temperatures. Since the DTS data show somewhat cooler temperatures than the P-T survey, we infer that the borehole had not yet achieved equilibrium following cold-water slug injection. We also note the effect of thermal inertia on the P-T survey tool, with the upgoing measurements showing consistently higher temperatures than the downgoing measurements, suggesting a high degree of uncertainty in the measurements collected with this tool.

Data analysis/interpretation

Borehole/reservoir flow. DTS records the borehole temperature recovery as a function of time and depth, as seen in Figure 5, for a period of eight days following cold-water injection. We observe maximum borehole temperatures of approximately 160°C centered near 265 m depth, with an isothermal zone approximately

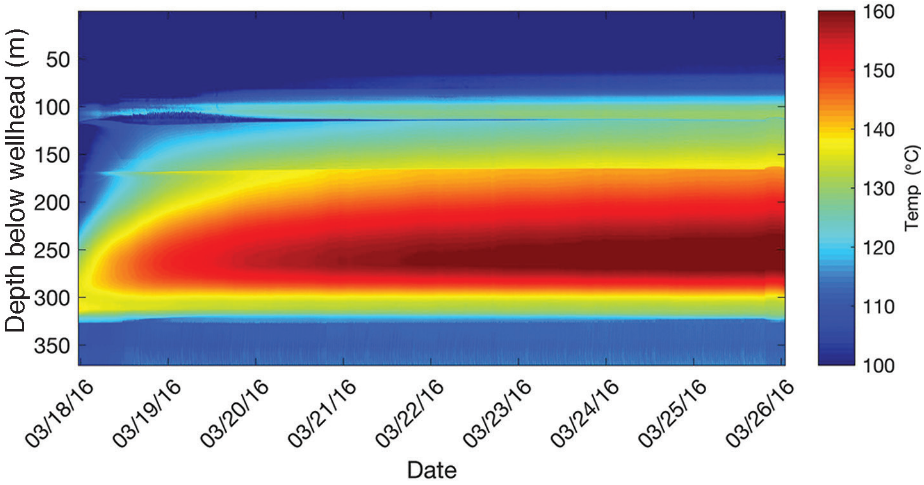

Figure 5. Depth profile temperature time series showing borehole temperature recovery following a cold-water slug injection into well 56-1. A maximum temperature zone approximately 50 m in thickness is centered at 250 m depth. An inverse temperature gradient begins at approximately 275 m, terminating in a persistent cold zone below approximately 325 m depth.

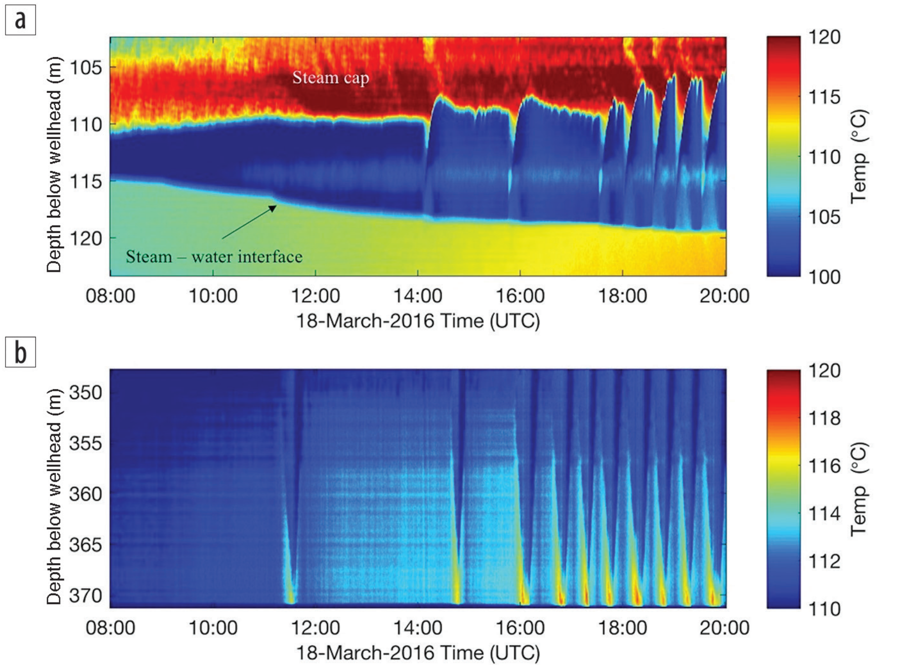

Figure 6. A 12 hour time series collected 18 March 2016. (a) The steam-water interface increases in depth with increasing time. The onset of phase change at the interface occurs as water level decreases resulting in depressurization. (b) The first evidence of forced convection into the open interval below 350 m depth is seen approximately 11 hours after the onset of pumping with evolution of periodic convection pulses occurring at 30 minute intervals.

50 m in thickness (Figure 5). The average geothermal gradient through the fluid-filled portion of the borehole (starting at ~125 m depth) to the maximum temperature zone is 0.23°C/m. Borehole cooling begins at approximately 265 m, with an average geothermal gradient of –0.78°C/m, over a thickness of approximately 60 m (i.e., ~325 m depth), where a stable cool zone exists to a depth of 372 m. The negative gradient observed below 265 m, which would not be expected under natural conditions, likely represents host rock cooling surrounding a dominant flow path, where heat is being extracted for active geothermal production within the Brady reservoir.

The temperature data provide further evidence for a dominant flow path near the bottom of well 56-1. The P-T survey before DTS cable installation clearly shows increases in temperature and pressure gradients, associated with being below water, at about 120 m depth. Without flow into the formation, we expect a 15 m^3 slug of water into well 56-1 to produce an initial water level change of approximately 52 m in the borehole, based on casing radii from the well construction. However, DTS data collected approximately seven hours after slug injection show no evidence of an elevated water level. Since the well is cased down to approximately 310 m depth, we infer that most or all water added to 56-1 exited the borehole below 310 m depth over a period of seven hours, implying a high-permeability zone (possibly associated with driller-designated fault zones) below this depth. Despite the expected change in water level, the water slug clearly cooled the borehole. We interpret temperature evolution to be thermal diffusion as heat flows from the hot rock toward the cool borehole, with temperature recovery measured by DTS (Figure 5).

DTS data clearly capture temperature variations over time scales on the order of an hour in well 56-1 during the borehole temperature recovery. We observe increased temperature pulses starting at approximately 350 m depth and moving to a depth of 372 m. Figure 6b shows the increased temperature pulses which began at approximately 11:30 UTC on 18 March 2017, about 11 hours after the beginning of stage 3 and the resumption of pumping operations at Brady. The pulses occur approximately every 30 minutes and are consistently 10 minutes in duration. Converting the temperature time series into an animation (see supplemental material at https://library.seg.org/doi/suppl/10.1190/tle36121024a.1), we also note pulses of decreased temperature in the animation at a depth of 120 m moving to the top of the borehole (Figure 6a). The decreased temperature pulses are first observed at approximately 14:30 UTC, roughly 14 hours after pumping resumed at Brady. DTS data also show a sharp temperature contrast at 115 m, which is interpreted to be the water level, with the abrupt temperature change at this level being the result of latent heat effects at the steam-water interface. This temperature contrast continues to decline in elevation throughout the time series (Figure 6a). This decline mirrors water level changes measured by a pressure sensor in monitoring well 56A-1, which is separated by a horizontal distance of 50 m and drilled to a similar depth as well 56-1; therefore, we infer that these wells are hydraulically connected.

We interpret the pulsing described earlier through the following mechanism. After pumping resumed at Brady, the pressure at the screened end of well 56-1 dropped, resulting in flow of water out of the cased well into the formation. This loss of water resulted in a drop of the water level in the well, decompressing the trapped steam column above 115 m and promoting further boiling. Pulses of water lost out of the bottom of the well thus may have produced pulses of pressure changes, causing further flashing of water to steam. This decompression boiling behavior and observed oscillating temperature signal is very similar to observations of decompression-related geyser eruption as discussed in a recent review of geyser eruption mechanics (Hurwitz and Manga, 2017).

The outflow of water out of the bottom of the borehole represents the only apparent exchange of water with the surrounding formation. However, changes in temperature within the cased section of the borehole (from ~130 to 300 m below the wellhead) are clearly apparent throughout the experiment. The borehole overall is heated throughout the period of 18–26 March as the borehole equilibrates with the surrounding hot reservoir rock. The strong temperature gradient between the borehole itself and the surrounding reservoir rock implies that most heat transfer is in the radial direction toward the borehole due to thermal diffusion. In the next analysis, we make the simplifying assumption that thermal diffusion in the radial dimension represents the dominant process within the cased borehole interval, and we use a numerical model to analyze the amount of heat diffusion at different depths within the borehole. The assumption of limited heat movement within the borehole (as would be caused by convection and forced advection) is revisited based on the analysis results.

Heat diffusion (cased borehole). To interpret the DTS data, we develop a numerical heat-transfer model to simulate temperature evolution within the borehole. We then use this model during inversion to estimate the depth profile of reservoir thermal diffusivity throughout the fluid-filled and cased portion of well 56-1 (130–300 m depth). The 1D radial heat-transfer model uses a finite-difference approach — center difference in space and implicit time stepping — to balance heat fluxes across individual finite-difference cells. A constant-temperature boundary condition is placed 2 m from the borehole center, and a zero-flux boundary condition is placed at the center of the borehole. Initial temperature is specified for fluid within the borehole. A representative value of thermal diffusivity for water (1.45×10^{-6} m^2/s) is selected to represent borehole fluid. The model assumes that heat transfer through forced and natural convection is small relative to heat diffusion and can be ignored. The model also assumes that most heat flow is occurring in a radially symmetric manner toward the borehole walls due to the large temperature gradients between the cooled borehole and warmer surrounding host rock. Similarly, the model assumes no vertical heat flow within the borehole or the reservoir. Fourier's law of heat conduction is used as the basis to build a linear system of heat-flow equations. We formulate and then solve the system of equations implicitly using Matlab's direct matrix solver.

Using the described model, we invert for host rock thermal diffusivity by minimizing misfit between modeled and observed data for each 1 m interval individually. The estimated parameters include: thermal diffusivity and initial temperature at each borehole depth independently in 1 m increments throughout the fluid-filled and cased portion of the borehole (130–300 m below wellhead), with no a priori information or regularization applied. We use the entire time series for each depth (11,235 data points per depth) with a direct-search optimization based on the Nelder-Mead simplex algorithm to minimize the sum of the squared residuals and determine the optimal thermal-diffusivity estimates.

Heat-transfer model and parameter estimation. We use the transient DTS data at individual depths to estimate the thermal-diffusivity depth profile in well 56-1. The results of the parameter estimation are shown in Figure 7, which includes the depth profile of thermal-diffusivity estimates, along with observed data and modeled data fit at the median diffusivity values for each lithology (144 m, 196 m, and 293 m). There are two major changes in thermal diffusivity seen in the depth profile, at 158 m and 285 m depth. The diffusivity changes that are seen closely correlate with

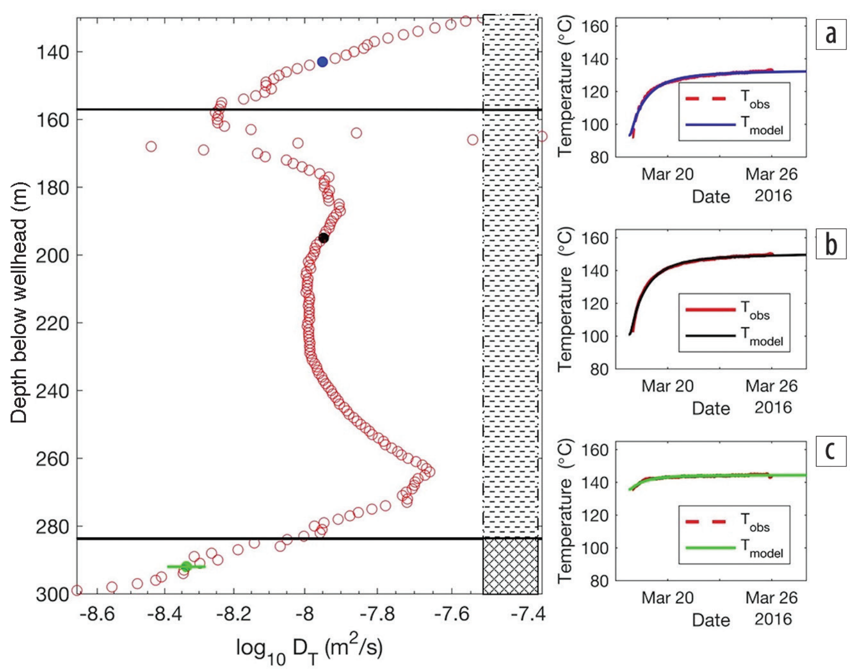

Figure 7. Vertical profile of thermal-diffusivity estimates throughout the fluid-filled and cased portion of the Brady observation well. Horizontal black lines represent lithologic contacts identified in geologic modeling efforts by Siler et al. (2016). Modeled data fit shown at representative depths: (a) 144 m, (b) 196 m, and (c) 293 m. Parameter uncertainty increases with depth. Error bars are present for all three representative depths, but are within circle radii for the upper two locations.

stratigraphic boundaries defined by geologic modeling (Siler et al., 2016). In conjunction with the large changes seen at 158 m and 285 m, we observe a trend of consistently decreasing diffusivity estimates starting at 265 m depth, the depth at which the inverted thermal gradient originates (Figure 5).

The median diffusivity estimates for each lithologic zone are 1.12×10^{-8} m^2/s at 143 m depth, 1.13×10^{-8} m^2/s at 196 m depth, and 4.61×10^{-9} m^2/s at 293 m depth (Figure 7). These values are lower than laboratory-measured values for lacustrine sedimentary rocks (1.3×10^{-6} m^2/s) and basalts (9×10^{-7} m^2/s); however, it is reasonable that the lacustrine sedimentary units have a higher median diffusivity value than that of the crystalline basalts. We hypothesize that the difference in lab-measured and our estimated diffusivity values is due to temperature dependence. It has been shown that diffusivity decreases with increasing temperature in a nonlinear manner, which could explain this discrepancy (Robertson, 1988).

We attribute the increasing variability seen at depths below 280 m to larger uncertainties in the diffusivity estimate. Although we have not conducted a rigorous uncertainty analysis, the 95% confidence interval for the median diffusivity increases with increasing depth. The increasing uncertainty is related to the decreasing temperature range of the fitted data at greater depths within the borehole (Figure 7).

Despite the temperature dynamics occurring at the top and bottom of the borehole as seen in Figure 6, we see no evidence of borehole convection upon detailed inspection of the collected data. The thermal-diffusivity estimates obtained support our assertion that radial heat diffusion into the borehole is the dominant heat-transfer mechanism due to temperature gradients between the borehole and surrounding reservoir rock. We expect estimated thermal diffusivity would be higher than reported lab values if other heat-transfer mechanisms (e.g., advection) were influencing borehole recovery. One example of this phenomenon occurs at approximately 165 m depth where we observe borehole temperatures recover more quickly compared to surrounding depths (Figure 5). We also note more highly variable diffusivity estimates surrounding this depth, including the highest diffusivity estimates throughout the depth profile (Figure 7). We infer that this signifies that heat transfer is occurring through conduction as well as advection, meaning that our effective diffusivity estimates are biased upward. We suspect this is due to a weak section in the casing; however, borehole images are not available to confirm this. We speculate this advection imprint would be seen through a wider range of depths if convective borehole processes or advection within the reservoir was a prominent heat-transfer process.

Conclusion

We have demonstrated the ability of DTS in a geothermal setting to provide data that capture spatiotemporal temperature dynamics in boreholes that are not seen with the more commonly used P-T surveys through the implementation of a thermal-response test. As seen in previous studies, this high spatiotemporal resolution can show dynamics that are difficult to capture with other methods, such as the pulsing seen in our study and the associated interesting borehole dynamics related to decreased pressures and steam flashing.

The thermal-response test conducted at Brady is different from other thermal-response testing in that the temperature perturbation is induced through a cold-water slug injection to cool the borehole as opposed to using electrical current to warm the borehole. The ability of DTS systems to capture the temperature transients in near real time allows us to estimate thermal diffusivity throughout the cased and fluid-filled portion of the borehole. Thermal characterization allows us to identify regions in the borehole that are warming more quickly, likely due to advection, which could indicate a weak section in the casing. By comparing thermal-diffusivity estimates to established lab values, we conclude that heat conduction is the dominant heat-transfer process during borehole recovery at Brady. This information provides useful evidence to site operators, demonstrating that flow and advection within the reservoir appears to be minimal outside of the faulted zones.

The information provided by our DTS survey provides a series of conclusions that would be valuable to site operators at geothermal sites including: (1) geothermal pumping produces water level changes and steam flashing, demonstrating that this well is hydraulically connected to pumping wells; (2) throughout the majority of the borehole, heat appears to be transported only via conduction, suggesting that the sole hydraulic connection between this well and production wells is along faulted intervals; and (3) application of a heat-transfer model provides estimates of thermal diffusivity throughout the reservoir, which could be useful for follow-on modeling of reservoir sustainability. This better understanding of both flow pathways and the distribution of thermal diffusivity throughout the reservoir allows plant operators to determine areas of the reservoir which will be the most thermally productive, as well as develop a sense of long-term thermal drawdown and financial sustainability of the reservoir. TLE

Acknowledgments

The authors wish to acknowledge the generous contributions of ORMAT Technologies who provided site access for installation of fiber-optic DTS systems at the Brady Geothermal Field. The authors also acknowledge expertise and thought-provoking questions provided by Doug Miller of Silixa Ltd. Finally, the authors would like to thank Baishali Roy, Jonathan Ajo-Franklin, and one anonymous reviewer for thoughtful feedback which greatly improved the quality of this paper. This research was supported by grants DE-EE0005510 and DE-EE0006760 from the U.S. Department of Energy Geothermal Technologies Office.

Corresponding author: jpatterson7@wisc.edu

References

Ali, S., J. Akerley, E. Baluyut, M. Cardiff, N. Davatzes, K. Feigl, W. Foxall, et al., 2016, Time-series analysis of surface deformation at Brady Hot Springs Geothermal Field (Nevada) using interferometric synthetic aperture radar: Geothermics, **61**, 114–120, https://doi.org/10.1016/j.geothermics.2016.01.008.

Bense, V., T. Read, O. Bour, T. Le Borgne, T. Coleman, S. Krause, A. Chalari, M. Mondanos, F. Ciocca, and J. Selker, 2016, Distributed temperature sensing as a downhole tool in hydrogeology: Water Resources Research, **52**, no. 12, 9259–9273, https://doi.org/10.1002/2016WR018869.

Coleman, T., 2016, PoroTomo DTS raw data: https://doi.org/10.15121/1367868.

Coleman, T. I., B. L. Parker, C. H. Maldaner, and M. J. Mondanos, 2015, Groundwater flow characterization in a fractured bedrock aquifer using active DTS tests in sealed boreholes: Journal of Hydrology, **528**, 449–462, https://doi.org/10.1016/j.jhydrol.2015.06.061.

Feigl, K. L., and P. Team, 2017, Overview and preliminary results from the PoroTomo project at Brady Hot Springs, Nevada: Poroelastic tomography by adjoint inverse modeling of data from seismology, geodesy, and hydrology: Presented at 42nd Workshop on Geothermal Reservoir Engineering.

Freifeld, B. M., S. Finsterle, T. C. Onstott, P. Toole, and L. M. Pratt, 2008, Ground surface temperature reconstructions: Using in situ estimates for thermal conductivity acquired with a fiber-optic distributed thermal perturbation sensor: Geophysical Research Letters, **35**, no. 14, https://doi.org/10.1029/2008GL034762.

Hurwitz, S., and M. Manga, 2017, The fascinating and complex dynamics of geyser eruptions: Annual Review of Earth and Planetary Sciences, **45**, no. 1, 31–59, https://doi.org/10.1146/annurev-earth-063016-015605.

Ikeda, N., K. Uogata, S. Kawazoe, and K. Haruguchi, 2000, Delineation of fractured reservoir by transient temperature analysis using fiber optic sensor: Presented at World Geothermal Congress.

Leaf, A. T., D. J. Hart, and J. M. Bahr, 2012, Active thermal tracer tests for improved hydrostratigraphic characterization: Groundwater, **50**, no. 5, 726–735, https://doi.org/10.1111/j.1745-6584.2012.00913.x.

Read, T., V. Bense, R. Hochreutener, O. Bour, T. Le Borgne, N. Lavenant, and J. Selker, 2015, Thermal-plume fibre optic tracking (T-POT) test for flow velocity measurement in groundwater boreholes: Geoscientific Instrumentation: Methods and Data Systems, **4**, 197–202, https://doi.org/10.5194/gi-4-197-2015.

Read, T., O. Bour, V. Bense, T. Le Borgne, P. Goderniaux, M. Klepikova, R. Hochreutener, N. Lavenant, and V. Boschero, 2013, Characterizing groundwater flow and heat transport in fractured rock using fiber-optic distributed temperature sensing: Geophysical Research Letters, **40**, no. 10, 2055–2059, https://doi.org/10.1002/grl.50397.

Robertson, E. C., 1988, Thermal properties of rocks, https://pubs.usgs.gov/of/1988/0441/report.pdf, accessed 1 August 2017.

Sakaguchi, K., and N. Matsushima, 2000, Temperature logging by the distributed temperature sensing technique during injection tests: Presented at World Geothermal Congress.

Sellwood, S. M., D. J. Hart, and J. M. Bahr, 2015, An in-well heat-tracer-test method for evaluating borehole flow conditions: Hydrogeology Journal, **23**, no. 8, 1817–1830, https://doi.org/10.1007/s10040-015-1304-8.

Siler, D. L., N. H. Hinz, J. E. Faulds, and J. Queen, 2016, 3D analysis of geothermal fluid flow favorability; Brady's, Nevada, USA: Presented at 41st Workshop on Geothermal Reservoir Engineering.